1986

Time scales and structure of topographic Rossby waves and meanders in the deep Gulf Stream

W. E. Johns
University of Rhode Island

D. Randolph Watts
University of Rhode Island, randywatts@uri.edu

Citation/Publisher Attribution
Johns, W. E., & Watts, D. R. (1986). Time scales and structure of topographic Rossby waves and meanders in the deep Gulf Stream. *Journal of Marine Research, 44*(2), 267-290. doi: 10.1357/002224086788405356
Available at: http://dx.doi.org/10.1357/002224086788405356

Journal of Marine Research, 44, 267–290, 1986

Time scales and structure of topographic Rossby waves and meanders in the deep Gulf Stream

by W. E. Johns[1,2] and D. R. Watts[1]

ABSTRACT

During July–November 1982, current and temperature records were collected from six current meters spanning the lower 2000 m of the water column on two moorings in the Gulf Stream northeast of Cape Hatteras, N.C. Frequency domain EOF analysis of the velocity cross-spectra reveals that there are two kinematically distinct wave processes present in the subinertial range, identifiable as topographic Rossby wave and meander-associated motions, which are energetically dominant at periods longer than and shorter than 14 days, respectively.

Simultaneous thermocline depth measurements obtained using inverted echo sounders show that the low-frequency topographic Rossby wave motions are uncoupled with near-surface displacements of the Gulf Stream path, but that cross-stream velocity fluctuations in the 14-day and 5-day period bands are associated with vertically coherent meanders of the Gulf Stream temperature front.

1. Introduction

It has been known for many years that velocity and temperature fluctuations in the upper layers of the Gulf Stream east of Cape Hatteras are dominated by periodic meanderings of the basic current structure on time scales of weeks to months. The characteristic zonal coherence scales of these meanders are sufficiently large that investigators have been able to successfully track their progression, using a variety of techniques, and to estimate with reasonable accuracy their downstream propagation speeds and growth rates (Hansen, 1970; Watts and Johns, 1982; Halliwell and Mooers, 1983).

Although hydrographic sections across the Gulf Stream east of Cape Hatteras typically show a baroclinic structure that extends throughout the water column, neither the deep mean current structure nor, particularly, the time-varying structure of the deep currents are known. Observations near 55W indicate a highly structured deep current variability with a local kinetic energy maximum beneath the Gulf Stream (Schmitz, 1978), which is, however, unclearly related to the near-surface Gulf Stream

1. Graduate School of Oceanography, University of Rhode Island, Narragansett, Rhode Island, 02882, U.S.A.

2. Present Address: Rosenstiel School of Marine and Atmospheric Science, Department of Meteorology and Physical Oceanography, University of Miami, Miami, Florida, 33149, U.S.A.

flow (Hendry, 1982). Near 63W, Kelley *et al.* (1982) correlated meridional excursions of the Gulf Stream system inferred from satellite imagery with deep current measurements and found that fluctuations with periods near two weeks influenced the entire water column, although again the exact nature of the vertical coupling was unclear. Recent observations from a single mooring near 68W (Hall and Bryden, 1985) indicate that the Gulf Stream does in fact extend coherently to the bottom, and that downstream flow events in deep water are associated with lateral shifts of the mid-thermocline current structure.

Farther upstream, approaching Cape Hatteras, where the Gulf Stream flows over more strongly sloping topography, there is conflicting evidence concerning the structure of deep velocity fluctuations. While certain short-term records indicate that Gulf Stream meanders extend coherently to the bottom (Robinson *et al.*, 1974; Schmitz *et al.*, 1970), it has become apparent in recent years that the deep water energetics over the continental rise are dominated by topographic Rossby waves with frequencies similar to those of growing meanders (Hogg, 1981; Thompson, 1977) but which have completely different phase properties and relatively short 0(50 km) zonal coherence scales (Luyten, 1977). The extent of the vertical coupling between upper and lower layers in the Gulf Stream therefore remains an open question.

We describe herein a new approach to the problem which is made possible by utilizing inverted echo sounders (IESs) together with deep current meters in a coherent array. This combination of instruments allows us to examine the deep current and temperature fluctuations in conjunction with continuous, accurate thermocline-level Gulf Stream path information. It will be shown that there is a vertically coherent deep velocity structure associated with Gulf Stream meanders, which is kinematically distinct from the bottom-trapped structure of the energetic, low-frequency topographic Rossby wave disturbances. The transition between these two wave regimes, occurring near periods of 12–16 days, is consistently evident in the kinematic and vertical structure as well as phase properties of the fluctuations.

2. Observations

During July–November 1982, 135-day records were obtained from an array of three inverted echo sounders (IESs) and six current meters deployed in the Gulf Stream 150 km northeast of Cape Hatteras, N.C. These measurements supplement an earlier data set collected during 1979-80 in this same region (Johns and Watts, 1985; hereafter JW85), but were designed to sample a larger extent of the deep water column than had been done previously. It was hoped that, by combining measurements of the variation in the depth of the main thermocline (using IESs) with deep current meter observations, one could determine whether meanders extend coherently to the bottom in this region, and, if so, begin to examine in more detail their kinematics and vertical structure. This paper discusses primarily the most recent set of observations, which are a subset of a larger experiment encompassing these separate deployments with records spanning a total of over 18 months.

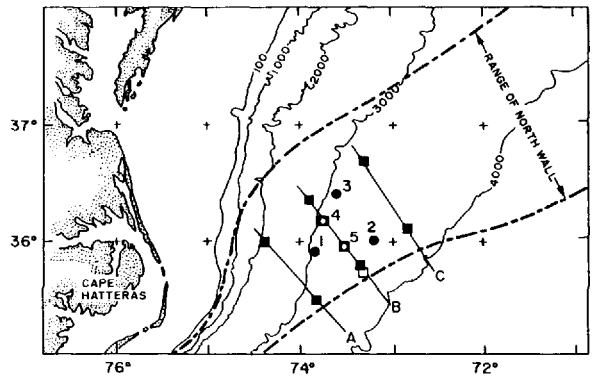

Figure 1. Survey area. Squares indicate the IES locations, and circles indicate the current meter mooring locations. Closed symbols designate the 1979–80 deployments; open symbols designate the 1982 deployments. The historical envelope of meandering of the Gulf Stream north wall is indicated by the bold dashed lines.

The IES/current meter array was placed within the historical envelope of meandering of the Gulf Stream in a region where meanders are known to exhibit rapid spatial growth, yet where the lateral excursions of the Stream are still small enough that the array could continuously monitor variations within the current. The instrument locations are shown in Figure 1. Current meters were placed at distances of 500, 1000, and 1500–2000 m off the bottom on each of two moorings, designated sites 4 and 5. All current meters were of the vector-averaging type (VACMs). The two moorings were spaced approximately 30 km apart, along a line perpendicular to the mean path of the Gulf Stream. This spacing was chosen to be less than the internal Rossby deformation radius (~40 km), based in part on the relatively weak coherence observed over a 50 km cross-stream separation in the earlier current meter records (sites 2 and 3, Fig. 1). The IES sites were chosen to monitor fluctuations in the depth of the main thermocline, associated with the meandering of the path of the Gulf Stream. IES measurements were taken directly at the two current meter sites 4 and 5, with an additional IES placed approximately 25 km offshore of site 5 to ensure good tracking of the Gulf Stream. A detailed verification of the IES technique in the Gulf Stream and a methodology for using these data to infer meander propagation and growth is described in Watts and Johns (1982).

The velocity and temperature time series measured at each of the current meters on moorings 4 and 5 are shown in Figure 2. All of the data records have been low-pass filtered with a 24-hour half-width Gaussian window, and then subsampled at 12-hour intervals. Thermocline displacement records obtained from IES measurements at moorings 4 and 5 are shown in Figure 3. Table 1 summarizes the current meter mooring locations, and the means and variances of the current and temperature records.

The velocity and temperature time scales range from a few days to about one month.

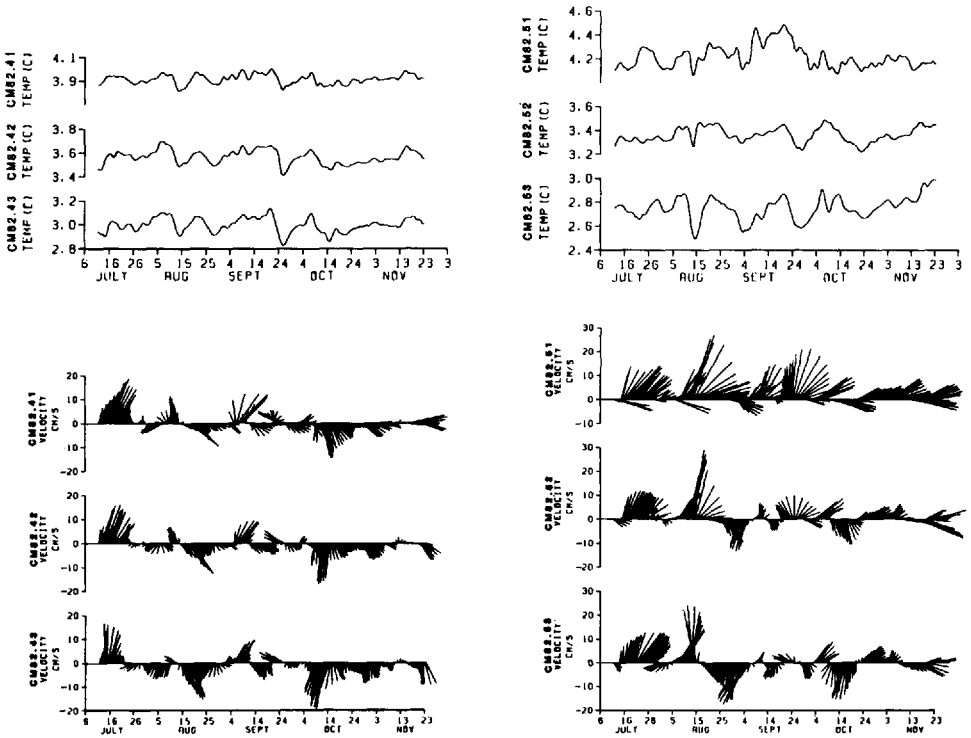

Figure 2. Time series of temperature and velocity (stick plots, with north up) at each of the current meter sites: mooring 4 (left) and mooring 5 (right).

For the most part, the velocity fluctuations appear to be highly coherent vertically, and several events occur in the records which can be traced horizontally between moorings 4 and 5. At least two of the more energetic events (near Aug. 25 and Oct 15) are bottom-intensified, although the true vertical structure of the fluctuations is somewhat obscured by the mean flow. For example, the event during late July, which appears nearly barotropic, is actually rather strongly bottom-intensified at mooring 5 after removing the mean vertical shear. During these events, current reversals at the upslope site (mooring 4) tend to lead those at the downslope site (mooring 5) by a few to several days.

3. Mean currents and energy spectra

a. Mean currents. The mean currents at sites 4 and 5 are illustrated in Figure 4, together with the means obtained from the earlier records at site 1 (for 6-months), site 2 (12-months), and site 3 (9-months) during the 1979–80 deployments. The most completely instrumented level is at 1000 m off the bottom, for which the mean currents are indicated in Figure 4 by solid vectors. A comparison with simultaneous thermocline

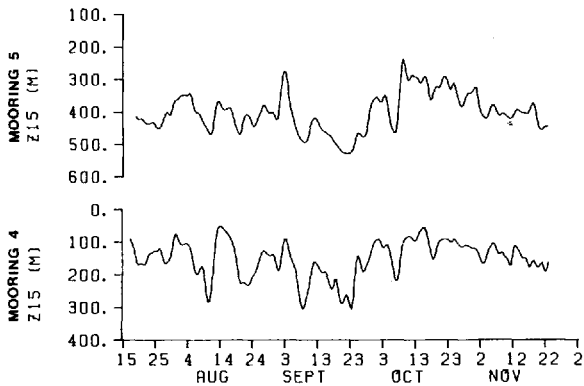

Figure 3. Time series of 15°C isotherm depth (Z15) at moorings 4 and 5.

depth measurements from the IESs shows that site 4 is moored almost directly beneath the mean location of the Gulf Stream's north wall (15°C at 200 m), whereas mooring 5 is farther offshore within the body of the Gulf Stream. At the actual current meter depths (>1200 m), however, both of these moorings are in the cyclonic shear zone of the deep Gulf Stream, due to the offshore tilt of the Gulf Stream's velocity structure with depth. Although some of the records are only about 4 months long, the mean currents obtained from the different measurement periods are remarkably consistent and present a clear picture of the deep flow field. At each of the three moorings in 3000 m water depth (moorings 1, 3 and 4) the mean current 1000 m off the bottom is veered to the right of the mean surface path (~050°T), whereas at mooring 2, in 3700 m water depth, the mean current 1000 m off the bottom is approximately colinear with the surface mean path. At mooring 5, in 3400 m water depth, the mean direction of flow 1000 m off the bottom is intermediate between these extremes. This offshore turning of the mean flow vectors suggests an inflow to the Gulf Stream which decreases systematically in strength in the offshore direction from a speed of about 3–4 cm s^{-1} near the northern edge of the Gulf Stream. The observed clockwise veering of the mean flow vectors with depth on moorings 4 and 5 further suggests that the inflow component is nearly barotropic, when subtracted from the vertically-sheared downstream component.

An interesting aspect of this vertical veering of the mean currents concerns its implication for vertical motion. While the cross-isobath orientation of the deep mean flow vectors kinematically implies some vertical component of flow down the slope, the observed vertical veering can be used to actually estimate the vertical velocity, based on the thermal-wind heat balance formulation of Bryden (1976). Following Bryden (1976), the advective heat equation

$$\frac{\partial T}{\partial t} + u\frac{\partial T}{\partial x} + v\frac{\partial T}{\partial y} + w\frac{\partial \bar{\theta}}{\partial z} = 0 + 0\{\nabla \cdot \overline{\mathbf{u}'T'}\} \tag{1}$$

Table 1. Summary of mooring information and current meter statistics.

Year-Site*	Latitude	Longitude	Duration (d)	Bottom Depth (m)	CM Depth (m)	Temp (°C) Mean	Temp (°C) σ	U (cm/s) Mean	U (cm/s) σ	V (cm/s) Mean	V (cm/s) σ
79-11	35°51.3′	73°50.2′	185	3070	1955	3.640	.058	4.2	3.8	−0.3	5.8
79-21	35°55.7′	73°13.7′	101	3690	2685	3.038	.073	2.5	2.7	1.6	4.7
80-21	35°55.8′	73°13.7′	241	3680	2665	3.127	.094	4.1	4.2	3.6	5.1
80-22	35°55.8′	73°13.7′	241	3680	3170	2.194	.066	0.6	3.4	0.8	2.8
80-31	36°18.0′	73°37.0′	241	3070	2060	3.489	.073	2.2	3.5	−1.2	5.6
82-41	36°10.0′	73°45.8′	135	3050	1420	3.916	.041	4.1	4.4	−0.4	6.0
82-42	36°10.0′	73°45.8′	135	3050	1955	3.565	.060	2.4	3.2	−1.6	5.8
82-43	36°10.0′	73°45.8′	135	3050	2490	2.997	.061	0.3	2.8	−3.2	6.4
82-51	35°57.3′	73°31.8′	135	3390	1230	4.215	.096	9.9	4.4	4.2	6.2
82-52	35°57.3′	73°31.8′	135	3390	2295	3.362	.064	4.8	4.2	−1.4	7.0
82-53	35°57.3′	73°31.8′	135	3390	2830	2.753	.096	2.0	4.3	−0.3	8.0

*The notation used for the current meter sites is a two-digit format, where the first number stands for the mooring number (1 to 5) and the second number denotes the current meter's position down from the top of that mooring (1 to 3). For example, site 42 is on mooring 4 and is second from the top.

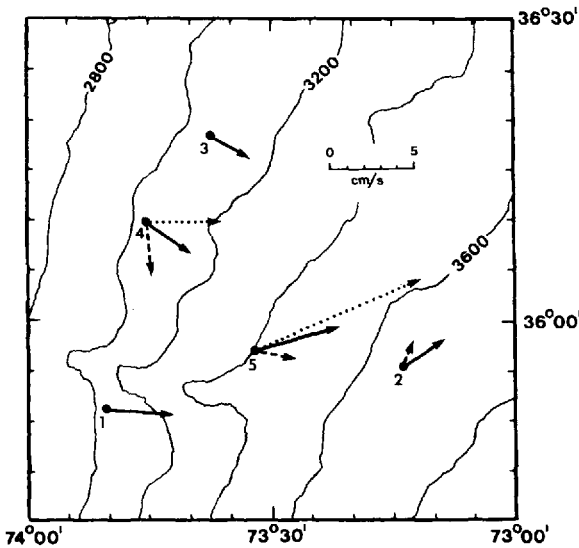

Figure 4. Mean currents. Dashed vectors indicate the means at 500 m off the bottom, solid vectors indicate the means at 1000 m off the bottom, and dotted vectors indicate the means at the shallowest levels (1500 m off the bottom at site 4 and 2000 m off the bottom at site 5).

may be written:

$$\frac{\partial T}{\partial t} + \frac{f}{g\alpha}\left(u\frac{\partial v}{\partial z} - v\frac{\partial u}{\partial z}\right) + w\frac{\partial \bar{\theta}}{\partial z} = 0 + 0\{\nabla \cdot \overline{\mathbf{u}'T'}\} \tag{2}$$

where α is an equivalent thermal expansion coefficient based on TS properties, and where the thermal-wind approximations $fv_z = g\alpha T_x$, $-fu_z = g\alpha T_y$, have been assumed. Alternatively, the above equation may be written as:

$$\frac{\partial T}{\partial t} + \frac{f}{g\alpha}\left(S^2\frac{\partial \phi}{\partial z}\right) + w\frac{\partial \bar{\theta}}{\partial z} = 0 + 0\{\nabla \cdot \overline{\mathbf{u}'T'}\} \tag{3}$$

by grouping the horizontal advection terms together under the transformation $u = S\cos\phi$, $v = S\sin\phi$, where S is the current speed and ϕ is the angle of flow measured counterclockwise from east.

We have used (2) to estimate the vertically-averaged local rate of change of temperature and horizontal advection of temperature at moorings 4 and 5 as a function of time, from which the means and standard deviations over the record have been computed (Table 2). The mean local rate of change of temperature is small (less than 1.0×10^{-8} °C s^{-1}), compared to the advective term, and is henceforth neglected. The mean horizontal advection of temperature at both moorings is large: 6.7×10^{-8} °C s^{-1} in the layer 500–1500 m off the bottom of mooring 4, and 3.1×10^{-8} °C s^{-1} in the layer 500–2000 m off the bottom at mooring 5. Interestingly, the standard deviations of

Table 2. Summary of heat balance calculations, showing the means and standard deviations of vertically averaged local rate of change of temperature ($\overline{T}_t$), horizontal advection of temperature ($\boldsymbol{u} \cdot \nabla_H T$) and estimated mean vertical velocity ($\overline{w}$), over various depth ranges on moorings 4 and 5. The terms are as defined in Eq. (2).

			$\boldsymbol{u} \cdot \nabla_H T(10^{-8}\,°\mathrm{C\,s^{-1}})$				
Mooring	Depth range	$\overline{T}_t$ (10^{-8} °C s^{-1})	Mean	Std. Dev.	Std. Dev. of Mean	$\overline{\theta}_z$ (10^{-5} °C cm^{-1})	$\overline{w}$ (cm s^{-1})
4	1420–1955 m	0.3 ± 0.6	7.5	15.1	4.1	0.66 ± .14	−.011 ± .007
	1955–2490 m	0.3 ± 0.7	5.8	15.1	4.1	1.06 ± .16	−.006 ± .004
	1420–2490 m	0.3 ± 0.6	6.7	15.1	4.1	0.86 ± .07	−.008 ± .005
5	1230–2295 m	0.6 ± 1.0	1.6	16.4	4.5	0.80 ± .11	−.002 ± .006
	2295–2830 m	0.9 ± 1.0	6.0	22.9	6.2	1.14 ± .21	−.005 ± .006
	1230–2830 m	0.7 ± 1.0	3.1	18.6	5.1	0.91 ± .08	−.003 ± .006

horizontal advection of temperature over the record length are generally only 2–4 times the mean values. Thus, if one assumes a 10 day integral time scale [a conservative estimate over the continental rise (Henry, 1982)], the mean horizontal advection of temperature at mooring 4 is significant (Table 2)—even for these relatively short records. Based on the measured $\overline{u'T'}$ and $\overline{v'T'}$ covariances (order 5.0×10^{-2} °C cm s^{-1}, Johns, 1984), and assuming a length scale of variation of approximately one Rossby internal deformation radius (~40 km), the maximum eddy heat flux divergence [right-hand side of (2)] could balance at most about one-third of this mean horizontal advection of temperature. Hence from (2), using the $\bar{\theta}_z$ values in Table 2, the downward mean vertical velocity needed to balance the observed mean horizontal advection of temperature is approximately 0.008 cms^{-1} at mooring 4 and 0.003 cms^{-1} at mooring 5. The observations therefore imply a strong mean downward motion of O(5–10 m d^{-1}) beneath the northern edge of the Gulf Stream, and also farther offshore (though somewhat weaker) beneath the core of the Gulf Stream. These results are qualitatively consistent with two-layer potential vorticity arguments proposed by Hogg and Stommel (1985), in which a deep southwestward flow (representative of the Western Boundary Undercurrent) turns eastward and crosses under the Gulf Stream by sliding down the topography in such a way as to conserve its layer thickness. However, based on historical data and recent deep current meter measurements along 36N (Casagrande, 1983), the present array (with the possible exception of the deepest level on mooring 4) should be well above and eastward of the Western Boundary Undercurrent. Due to the limited coverage of our current meter array it is not clear to what extent this apparently broader deep flow is actually crossing under the Gulf Stream, as would be consistent with a deep circulation scheme proposed recently by Hogg (1983), or whether the inflow might be associated with the western fringe of a deep slope water recirculation gyre similar to that calculated from inverse methods by Wunsch and Grant (1982) (their Fig. 15(b)). In the latter case the inflow may be thought of as adding deep transport to the Gulf Stream. If integrated over depth and over a 100 km segment of the path, the observed 3–4 cm s^{-1} inflow yields a transport of approximately 10×10^6 m^3 sec^{-1}, which implies that a significant fraction of the observed increase in transport of the Gulf Stream in this region (Knauss, 1969) may be entering from the north. These observations are consistent with Halkin and Rossby's (1985) 3-year average of 73W "Pegasus" measurements, from which they estimate a nearly barotropic northern inflow of 10.4×10^6 m^3 s^{-1} per 100 km segment of the path in the upper 2000 m, roughly twice their estimate of the transport entering the Gulf Stream within this same depth range from the recirculation region to the south.

b. Kinetic energy spectra. To examine the structure of the fluctuating currents, kinetic energy spectra were computed by breaking up the records into 48-day segments, removing the mean, windowing with a Hanning (cosine) window in the time domain,

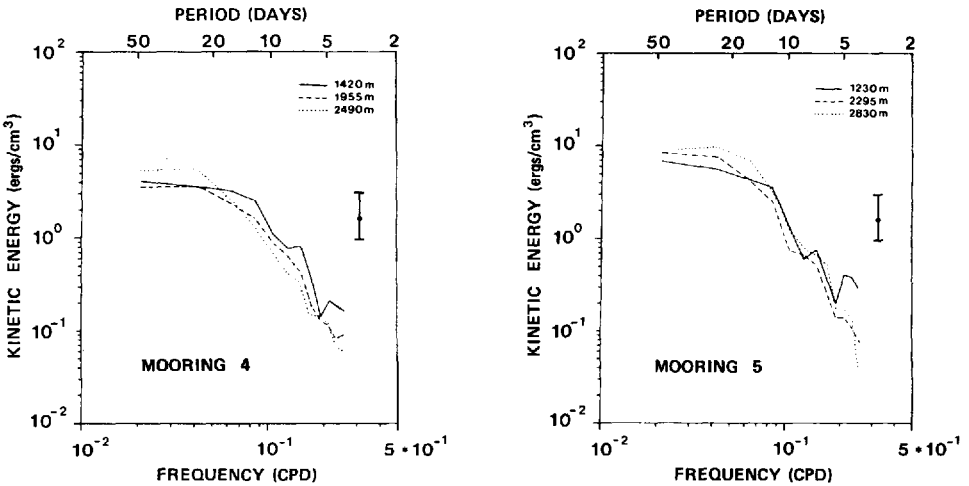

Figure 5. Eddy kinetic energy spectra at three depths on moorings 4 and 5.

Fourier transforming, and ensemble averaging. Segments were overlapped by 24 days (i.e., 50%). The resulting adjacent spectral estimates at periods of 48 d, 24 d, 16 d, etc. have effective bandwidths of 0.0312 c.p.d. (approximately 7 degrees of freedom) and are overlapped in the frequency domain by 33% (i.e., adjacent estimates are 67% independent). All additional spectral and cross-spectral quantities were computed in a similar manner. Some of these estimates (discussed later) have been averaged over two frequency bands to improve the reliability of estimates. These two-band-averaged estimates (approximately 12 degrees of freedom) are centered at periods of 32, 14, 8.8, 6.4, 5.1, and 4.2 days, and are nominally 83% independent. Much of the subsequent analysis in sections 3 and 4 deals with these six basic frequency bands spanning periods from 4 to 48 days.

Figure 5 illustrates the vertical distribution of kinetic energy at moorings 4 and 5. Both sites are characterized by an increase in kinetic energy with depth for periods longer than about 16 days. Near periods of 14 days, however, the structure changes. The kinetic energy in the 4- to 14-day period band at mooring 4 decreases with depth, and at mooring 5 the kinetic energy is nearly equal at the uppermost and deeper levels, but lower at the intermediate level. At both sites there is an obvious spectral 'bulge' near periods of 5 days at the upper levels which does not, however, appear at deeper levels. Aside from this, the spectra are rather featureless, except for the notably small spectral slopes occurring at low frequencies. In fact, at the deepest levels on moorings 4 and 5 the kinetic energy density is actually larger at the 24 day period than at the 48 day period. This trend toward dominance of the mid-frequency band is typical of current records taken on the continental slope and rise (c.f., Thompson and Luyten, 1976), as distinguished from the "red" structure observed in open-ocean, flat-bottom

regions where the kinetic energy is dominated by longer time scales, approximately 100 days (Richman *et al.*, 1977). Beginning near periods of 12–16 days and continuing to the 4-day period, all of the kinetic energy spectra fall off rapidly, with spectral slopes of f^{-2} to f^{-3}.

4. Velocity structure

To examine in more detail the structure of the velocity field we performed a frequency-domain, complex eigenvector (EOF) analysis on the current records (Groves and Hannan, 1968; Wallace and Dickinson, 1972). This analysis technique provides an efficient way to objectively analyze the complete body of simultaneous cross-spectral information for contributions from various wave structures.

In our earlier analysis of deep current meter records here (JW85) we found that the velocity fluctuations exhibited a consistent change in orientation with frequency: at low frequencies (periods >10 days) the fluctuations were aligned closely along the isobaths, whereas at higher frequencies the fluctuations were more isotropic but tended to be oriented across-stream. Figure 6 illustrates the principal axes of variance from both the earlier records (moorings 1–3), and from the new records (moorings 4 and 5), in two frequency bands. We suggested in JW85 that the cross-stream orientation is a signature of deep meander variability, and that the along-isobath flow at low frequencies is a manifestation of topographic Rossby wave variability. The following frequency-domain EOF analysis was designed to further test these hypotheses.

For any given frequency band, the cross-spectra between all possible pairs of n measured physical variables can be represented as an $n \times n$ Hermitian matrix: the diagonal elements are (real) auto-spectral estimates obtained by crossing each variable with itself, and the off-diagonal elements are (complex) cross-spectral estimates between pairs of variables. This cross-spectral matrix may be diagonalized to a linear combination of n orthogonal eigenvectors with weights λ_i (the associated real eigenvalues), which determine the fraction of the cross-spectral variance explained by the i^{th} eigenvector, or mode (Wallace and Dickinson, 1972).

Prior to diagonalization, the cross-spectral matrix is normalized by dividing each element by the product of the square root of the variance associated with each member of that pair. This is known as coherence normalization, which effectively nondimensionalizes the matrix (if variables with different physical units are used), and also has the advantage of giving equal weight to the measurements at each site. Otherwise the results are dominated by the few largest (most energetic) elements.

This procedure has been applied to the vector velocity time series at moorings 4 and 5. Temperature variations are considered separately in the next section, where they are compared with the simultaneous thermocline displacement records. There are a total of 12 velocity variables (east and north components measured at six locations). EOFs were computed for each of the six frequency bands centered at periods of 32, 14, 8.8,

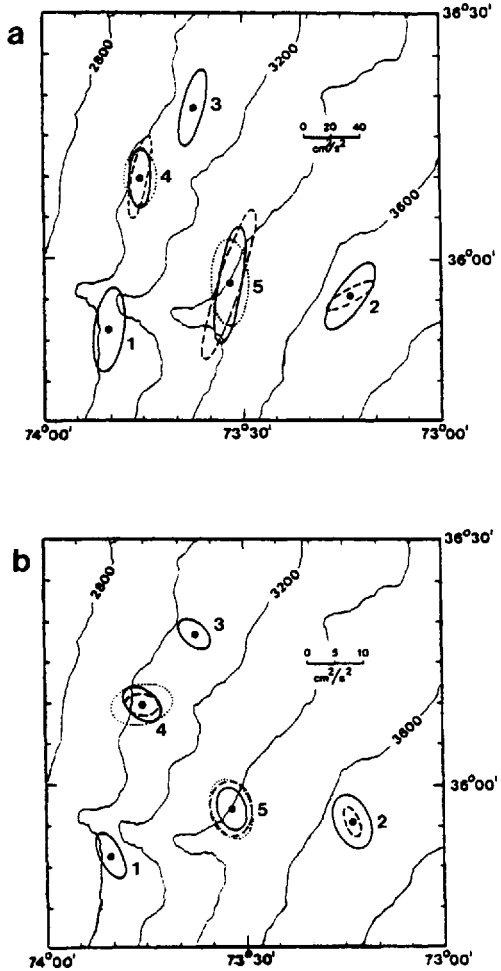

Figure 6. Rotary variance ellipses for each of the current meter sites: (a) 12–48 day band, and (b) 4–10 day band. Dashed ellipses indicate sites at 500 m off the bottom, solid ellipses at 1000 m off the bottom, and dotted ellipses at the shallowest levels (1500 m off the bottom at site 4 and 2000 m off the bottom at site 5).

6.4, 5.1, and 4.2 days. For each frequency band, there result 12 complex eigenvectors, $\tilde{\mathbf{e}}_i$:

$$\tilde{e}_i = [\tilde{u}_1^2, \tilde{u}_2^2, \ldots . \tilde{u}_{12}^2]$$

which express the variance of velocity components and relative phase differences between components for each mode. The fractional variance accounted for by the i^{th} mode is:

$$\lambda_i / \Sigma \langle u_j u_j \rangle$$

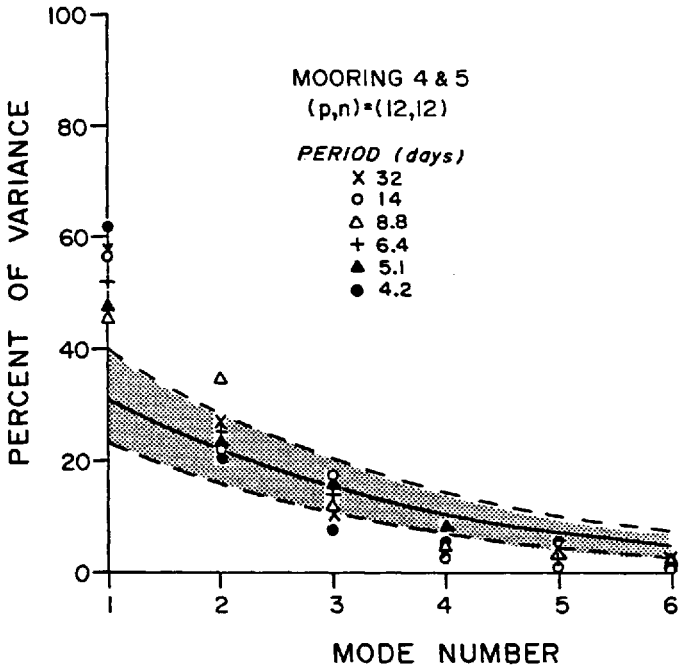

Figure 7. Percent of variance explained by successive EOF modes at moorings 4 and 5. The symbols designate modes in different period bands, as shown. The solid line is the "noise" eigenvalue distribution for 12 degrees of freedom, and the shaded area indicates the 5% to 95% confidence intervals of this distribution.

determined by the size of the i^{th} eigenvalue relative to the trace (total normalized variance, n) of the matrix.

The statistical significance of modes obtained by the EOF decomposition depends on the observed distribution of the λ_i relative to the standard probability distribution for λ_i based on a noise hypothesis, i.e., that of uncorrelated variables. Priesendorfer (1981) presents a comprehensive set of tables of the probability distributions for eigenvalues of random covariance matrices, as a function of n, the order of the matrix (number of variables), and p, the number of degrees of freedom associated with the matrix elements. The "noise" eigenvalue distribution for $(p, n) = (12, 12)$ is shown in Figure 7, where it is compared with the observed eigenvalue distribution (each two-band-averaged estimate has approximately 12 degrees of freedom). According to this test all 1st modes contain significant variance at the 95% level, as does the 2nd mode in the 8.8 day band. A more subjective but commonly used significance test is that the 1st mode should explain at least twice as much variance as the 2nd mode (Wallace and Dickinson, 1972). This test is perhaps more useful for dynamical interpretation and is satisfied here in all frequency bands except the 8.8. day band.

The basic quantities which describe a given mode are the magnitude of u and v at

each site, the phase between u and v at each site, and the relative phase between velocity components at different sites. These quantities are graphically represented in terms of velocity hodographs for each mode, shown in Figure 8, in which the modes have been re-dimensionalized by the corresponding spectral levels (see Appendix). For any given mode, this representation allows vertical and horizontal phase variations over the array to be expressed concisely in terms of the relative phase of the principal, or major axis, velocity component.

In the 32-day band, the first mode describes bottom-intensified fluctuations which are oriented along the bathymetry and are nearly in phase vertically. The motion has a cyclonic rotary tendency (i.e., u leads v), but becomes increasingly transverse with depth. There is a large energy variation apparent in the array, with about three times more kinetic energy accounted for by this mode at site 5 than at site 4. Importantly, there is an average phase offset of approximately 60° between moorings 4 and 5, such that fluctuations lead (occur earlier) at site 4.

In the 14-day band, the first mode describes fluctuations which are now oriented in the NW-SE quadrant, more nearly perpendicular to the mean path of the Gulf Stream. The fluctuations are in phase vertically and are essentially barotropic, with perhaps a slight upward intensification. At each site u and v are nearly out of phase, except at the deepest level on mooring 5 where the fluctuations are purely anticyclonic (v leads u by 90°) and the orientation is skewed N-S. This suggests that the fluctuations are weakly coupled vertically in deep layers at mooring 5. For this mode there is a much smaller (insignificant) average cross-stream phase offset of 12° between moorings 4 and 5.

At shorter periods, the cross-stream orientation continues to be dominant; however, the mode structures become generally noisier and there are often irregular variations in orientation and phase over the array. For example, in both the 8.8- and 6.4-day bands the cross-stream, vertically in-phase motion shows up strongly at one mooring but not at the other, and in the 4.2-day band the variance is dominated by cross-stream, horizontally in-phase motion at the upper levels but not at depth. In the 5.1-day band the cross-stream, transverse variability does occur as a coherent 1st mode throughout the array.

The variability at sites 4 and 5 can be summarized in terms of a transition from bottom-intensified flow oriented along the bathymetry at low frequencies, to essentially barotropic flow oriented in the NW-SE (cross-stream) direction at higher frequencies. The two coherent wave structures are further distinguished by the fact that the 32-day period fluctuations exhibit a significant phase lag over the 30 km cross-stream separation between sites, but that the cross-stream fluctuations at higher frequencies (periods of 14 days and 5 days) are nearly in-phase across the Gulf Stream. The 32-day period fluctuations are characterized by offshore propagation, while the in-phase variability at higher frequencies suggests wavefronts oriented in the cross-stream plane, implying alongstream propagation. These results are consistent with our earlier findings (JW85), which indicated offshore phase propagation at low frequen-

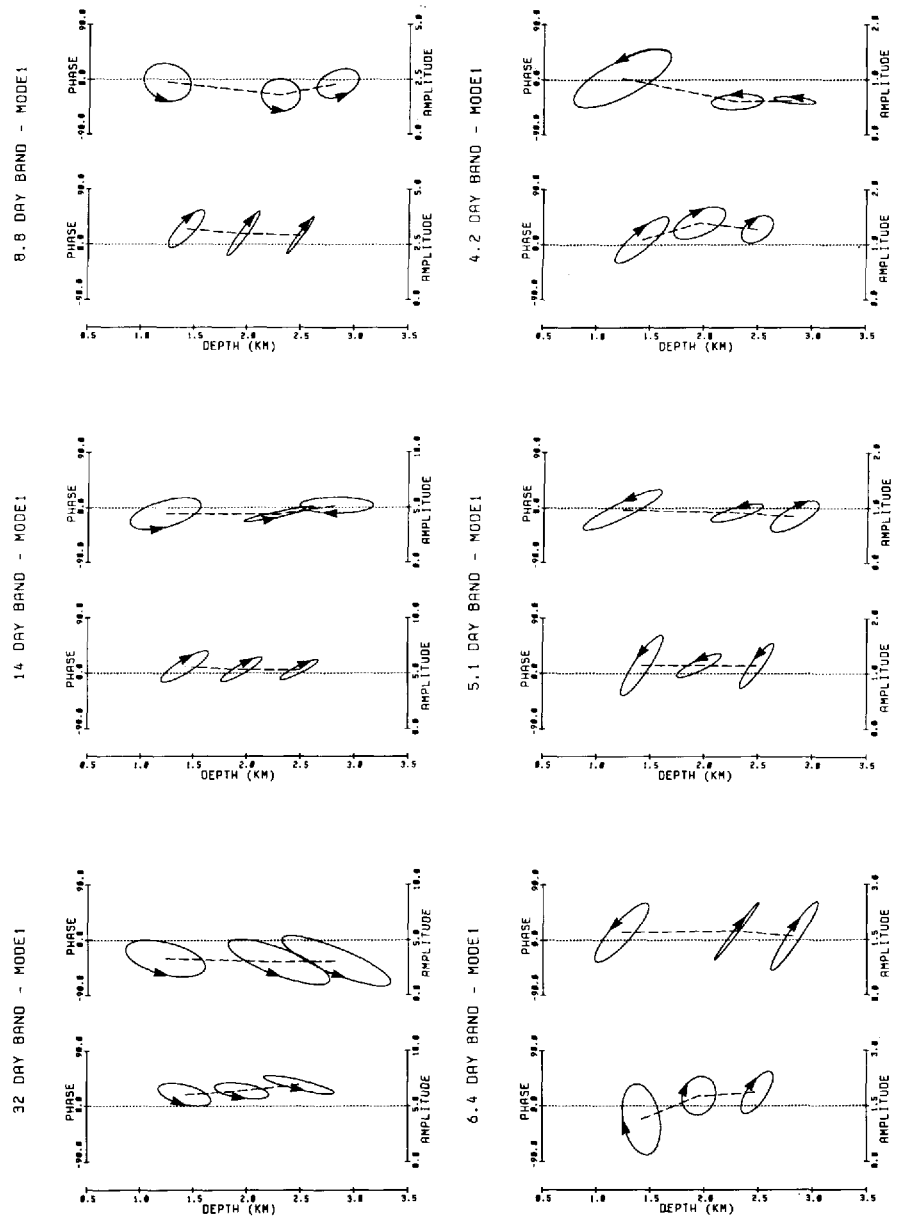

Figure 8. Structure of first EOF modes. Each frame illustrates the velocity hodographs at mooring 4 (left) and mooring 5 (right), within a particular period band. The geographical orientation and eccentricity of the velocity ellipse are displayed in the "plan view" sense, with north up and east to the right. The phase of the major axis velocity component at a site is indicated by the position of the center of the ellipse relative to the top axis. Amplitudes are in cm s^{-1}.

cies and downstream phase propagation for periods shorter than approximately 10 days.

The vertical structure, horizontal phase variation, and transverse character of the low-frequency fluctuations are very consistent with the kinematics and dispersion of topographic Rossby waves (TRWs). Rhines' (1970) linear topographic wave model showed that in the presence of both stratification and significant bottom slope the structure of low-frequency wave motions is bottom-intensified, with vertical structure of the form $\cosh(\kappa Nz/f)$, where $\kappa = (k^2 + \ell^2)^{1/2}$ is the horizontal wavenumber, N is the Brunt-Väisälä frequency, f is the Coriolis parameter, and z is measured upward from the bottom ($z = -H$). The frequency of this mode is given approximately by $\omega = \Gamma N \sin\theta$ where Γ is the bottom slope and θ is the angle between the wavenumber vector and upslope. The fluid velocity is in the plane of the wavefronts, so that in the low-frequency limit the velocity fluctuations should be transverse along the isobaths and in the high-frequency limit the fluctuations should be transverse up- and downslope. Observationally, the variance ellipses and wavenumber vectors are very nearly perpendicular (Thompson, 1977). For typical regional values $N = 10^{-3}$ sec^{-1} and $\Gamma = 10^{-2}$, the shortest period to be expected is about $2\pi/\Gamma N \sim 8$ days.

Thompson and Luyten (1976) showed previously that Rhines' (1970) model could accurately predict the orientation of the major axis of low-frequency variance ellipses at Site D (39°10′N, 70°W) as a function of frequency. Also, from the "Rise Array" data (Luyten, 1977), Thompson (1977) obtained good agreement between the model predictions and observed phase propagation of motions with periods from 8 to 32 days. Independently, Hogg (1981) analyzed the "Rise Array" data using EOFs and found that the horizontal phase variations and upward energy decay were well-described by a simple topographic wave propagating offshore and refracting slowly in response to changes in depth, bottom slope, and stratification. A summary of TRW properties estimated by Thompson (1977) is given in Table 3.

At sites 4 and 5, the mean orientation of the first mode ellipses in the 32-day band is 15°T, just about exactly parallel to our estimate of the orientation of the mean bathymetry (15°T and 20°T, respectively). The theoretical prediction for a 32-day topographic wave in the presence of bottom slope and stratification (Γ, N) = (10^{-2},10^{-3}sec^{-1}) is a clockwise rotation of $\theta = \sin^{-1}(\omega/\Gamma N) = 13°$ relative to the isobaths. Although small, this predicted rotation does not seem to be present in these records. It is worth noting, though, that the direction of the isobaths in this region is sufficiently irregular over small scales that accurate estimates of the dynamically significant topography are rather difficult to make, especially at site 5 (see Fig. 4). For bottom-trapped waves the ellipse orientation of 15° implies a wavenumber vector pointing along 105°T, which is approximately 30° off the line joining sites 4 and 5 (138°T). The 60° average phase offset between these sites, separated by $\delta y = 31.7$ km, therefore implies a phase speed $c = (1/T)(2\pi/\delta\psi)\,\delta y/\cos(30°) = 6.9$ km day^{-1} and wavelength $\lambda = 220$ km. These estimates compare favorably with the 7–8 km day^{-1}

Table 3. Observed topographic Rossby wave dispersion parameters on the western North Atlantic continental rise: period (T), wavelength (λ), phase speed (c), and angle (θ) between the wavenumber vector and downslope direction. For each period listed, the first row of numbers correspond to Thompson's (1977) Site "S" estimates, and the second row represents an average of Thompson's (1977) estimates from the "Rise Array" moorings in less than 3500 m water depth.

T (days)	λ (km)	c (km/d)	θ (deg)
32	230	7	15
	270	8	11
16	290	18	16
	160	10	27
11	140	13	37
	170	15	34
8	190	24	49
	160	20	47

phase speeds and 0(250 km) wavelengths for 32-day period TRWs reported in Table 3, all of which were estimated from measurements taken in regions with similar (Γ, N).

The vertical decay scale of the motion has been estimated from our observations by a least-square fit of the first-mode principal axis velocity components to the theoretical vertical structure $V = V_o \cosh(\alpha z)$. The decay scale, α, obtained in this way is 0.43 km^{-1} for site 4 and 0.37 km^{-1} for site 5. These estimates are somewhat larger than, but comparable to, the theoretical decay scale $\alpha = \kappa N/f = 0.33$ km^{-1}, based on the estimated 220 km wavelength.

The 32-day period motions are therefore consistent with the properties of topographic Rossby waves, the single exception being the lack of a characteristic clockwise rotation of the wavefronts relative to the isobaths. Despite the uncertainties in the topography this discrepancy seems to be real,[3] and the absence of the characteristic rotation may indicate the superposition of a coherent, cross-isobath motion similar to what is observed at higher frequencies, but which is energetically much weaker than the TRW signal at low frequencies. This impression is also given by the counterclockwise rotation of the low-frequency variance ellipses with height at moorings 4 and 5 (Fig. 6).

From earlier work we know that Gulf Stream meanders in this region are energetic over a range of periods from 4 days to at least 50 days (Watts and Johns, 1982; Halliwell and Mooers, 1983). Since TRWs have a high-frequency cutoff near 8 days, one would expect a meander-associated variability to emerge at periods shorter than about 8 days. In fact, the EOF analysis suggests that this transition occurs at significantly longer periods, around 14 days. It is important to note that for 14-day

3. The planetary β-effect cannot account for this, since it contributes an effective north-south bottom slope here of $\beta H/f \sim 10^{-3}$ to the f-plane dynamics and should therefore tend to force trajectories along slightly more zonally-oriented paths (as one would expect), opposite in sense to what is observed here.

period motions the TRW theory predicts a 25–30° clockwise rotation of the principal axes relative to the bathymetry, whereas the observed rotation is much larger than this, >90°. This abrupt transition to a cross-stream orientation suggests that the higher-frequency fluctuations are associated with vertically coherent lateral shifts of the Gulf Stream's path. In the next section we examine the vertical coherence and structure of the temperature field to test whether the cross-stream EOF velocity modes found in the 14- and 5-day period bands are, in fact, associated with vertically coherent meanders of the Gulf Stream temperature front. Secondly, we wish to examine the nature of the vertical coupling, if any, between the low-frequency bottom-intensified motions and near-surface displacements of the Gulf Stream path.

5. Temperature structure

Vertical displacements of the main thermocline at sites 4 and 5 are highly coherent and in phase for periods longer than about 4 days (Johns, 1984), and are associated with lateral displacements of the Gulf Stream path here of 10–15 km r.m.s. amplitude (Watts and Johns, 1982). The mean depth of the 15°C isotherm (Z15) at site 4 is 150 m, so, as mentioned previously, mooring 4 lies within 5 km of the record-mean position of the Gulf Stream's north wall. At site 5, approximately 25 km offshore of the record-mean north wall position, the mean Z15 is 400 m.

Figure 9 shows the coherence and phase between thermocline (15°C isotherm) depth fluctuations at sites 4 and 5 and temperature fluctuations at each level on moorings 4 and 5. The results are divided into four frequency bands (24–48, 12–16, 6–10, and 4–5 days) based on the results of the EOF analysis. Also shown in Figure 9 are the r.m.s. vertical displacement fields in each of these frequency bands. At each current meter site the r.m.s. vertical displacement in a given frequency band is obtained by dividing the standard deviation of *in situ* temperature within that same band by the local vertical potential temperature gradient, $\bar{\theta}_z$ ($\pm 15\%$), calculated from available "Pegasus" data (H. T. Rossby, personal communication).

Near the northern edge of the Gulf Stream (site 4), the coherence between thermocline displacements and temperature fluctuations at the uppermost level (1420 m) is significant in all frequency bands. Below this, at depths >2000 m, the coherence becomes insignificant in the 24–48 day band, but remains significant in each of the other frequency bands. What is immediately striking is the high coherence in the 12–16 day band throughout the entire water column. The coherence in the 4–5 day band is also quite high, relative to the significance level, and is considerably larger than in the 6–10 day band.

The phase estimates are consistently positive (20 to 40°) in the two lowest bands and consistently negative (-5 to -25°) in the two highest bands. However, only the positive phase estimates in the 12–16 day band are significantly different from zero at the 95% level (due to the high coherence), implying that in this frequency band, vertical displacements in the lower layer tend to lead those at the thermocline level.

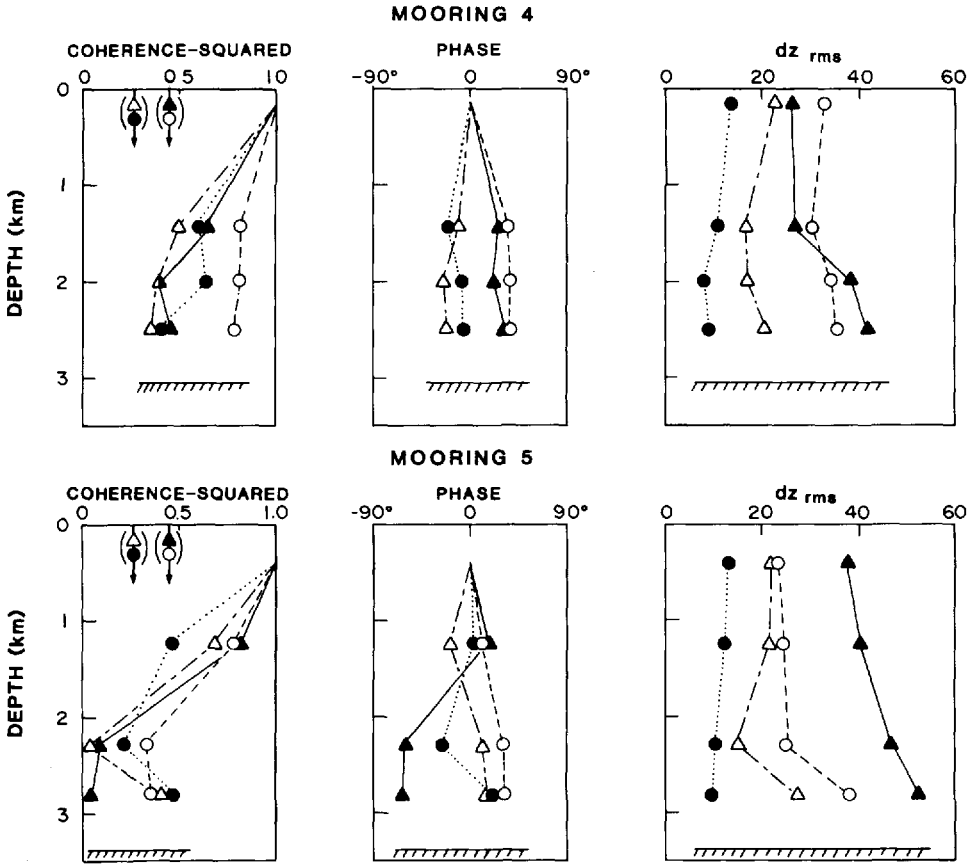

Figure 9. Coherence-squared and phase between thermocline depth fluctuations and temperature fluctuations at each level on moorings 4 and 5, and r.m.s. vertical displacement amplitudes. Each symbol represents a different period band: ▲, 24–48 days; ○, 12–16 days; △, 6–10 days; ●, 4–5 days. The 95% confidence level for non-zero coherence-squared in the 24–48 day and 12–16 day bands is 0.45; in the two higher bands (with greater bandwidth) it is 0.27, as indicated by arrows.

At mooring 4 there is an obvious bottom-intensification of the temperature signal in the 24–48 day band, with r.m.s. vertical displacements increasing by a factor of approximately 3/2 between the thermocline and 2500 m depth (500 m off the bottom). This corroborates the bottom-intensification observed in the 24–48 day velocity eigenfunction, as would be expected for topographic Rossby wave motions, which are in approximate geostrophic balance. In each of the higher-frequency bands the vertical displacement field becomes essentially barotropic.

Farther offshore, at mooring 5, temperature fluctuations are also significantly correlated with thermocline displacements at the uppermost level (1230 m), but below

this the vertical decay of the coherence function in all frequency bands is more rapid than at mooring 4. The low-frequency vertical displacements at the two deepest levels, again bottom-intensified, are totally incoherent with displacements at the thermocline level. Similarly, in the 12–16 day band, the vertical coherence is insignificant below 2000 m, remarkably different from that observed at mooring 4. Interestingly, there is evidence for bottom-intensification at periods as short as 6–10 days, which may imply an increased TRW influence at shorter periods in the deeper waters here.

Our earlier results (JW85) showed a similar offshore decrease of vertical coherence for fluctuations with periods less than about 16 days, but, in contrast to these measurements, showed significant vertical coherence of the low-frequency (24–48 day period) temperature field across the Gulf Stream. We point out, however, that the low-frequency cross spectra between near-surface path displacements and deep temperatures in the earlier records were dominated by a single large-amplitude meander apparently forced by interaction between the Gulf Stream and a warm-core ring (Cornillon, 1982), whereas the present records did not contain such an energetic low-frequency event. The correct interpretation may be simply that when large meanders do occur they extend coherently to the bottom, but that normally the low-frequency signals in deep water associated with evolving, small-amplitude meanders in this region are effectively masked by the energetic topographic wave variability. In any case, the low-frequency statistics are obviously not yet stationary and require further measurement.

The kinematics of the organized, one- to two-week time scale meandering motions may be understood by examining the phase relationship between the fluctuating velocity and temperature fields. At each of the current meter sites the coherence between temperature and cross-stream (positive northwest) velocity, shown in Figure 10, is peaked near the 5-day period and typically shows a secondary maximum near the 14-day period. The phase between temperature and cross-stream velocity is consistently positive (i.e., such that temperature leads), and is very near 90°, except at the deeper levels on mooring 5 where the phase estimates are considerably noisier and some tend toward 180°. In JW85 we discussed the significance of this phase relationship for propagating meanders and showed that in deep layers there exists an approximate three-term balance between local rate of change of temperature, cross-stream advection of temperature, and vertical advection of temperature, with the first two being of like sign. Thus, on average, vertical advection of temperature balances the sum of local rate of change and cross-stream advection of temperature. Kinematically this requires $|w/v| > |T_y/T_z|$, so that parcel trajectories in the cross-stream plane are inclined at angles steeper than the mean cross-stream slope of the isotherms. Physically, *onshore* displacements of the deep front are associated with *downward, offshore* advection of the deep isotherms, whereas *offshore* displacements are associated with *upward, onshore* advection of the isotherms. The meandering of the Gulf Stream thermal front is therefore a strongly three-dimensional process in which

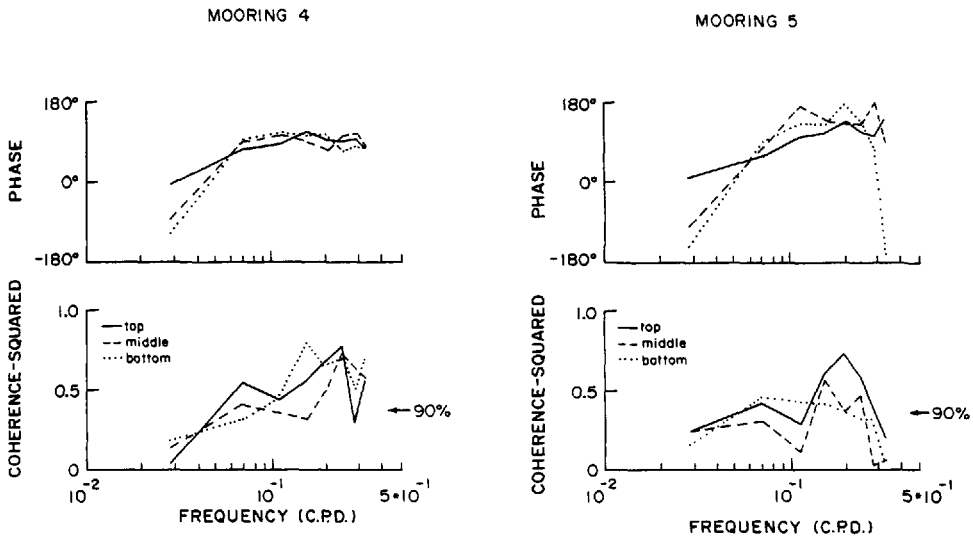

Figure 10. Coherence-squared and phase between temperature and cross-stream velocity at moorings 4 and 5. Solid lines, shallowest meters; dashed lines, 1000 m off the bottom; dotted lines, 500 m off the bottom.

vertical advection of heat is of leading order. The interested reader is referred to Johns and Watts (1985) for a more detailed mathematical treatment and analysis of the deep kinematic balances.

6. Conclusions

Based on our observations to date we offer the following summary of the current and temperature variability in this region. At levels shallower than ~1500 m, temperature variations in all frequency bands are dominated by spatially coherent displacements of the thermal structure, associated with the meandering of the path of the Gulf Stream. However, at low frequencies (periods of 24 to 48 days), the meander-dominated regime in the upper layer gives way to an essentially uncoupled topographic Rossby wave variability below about 2000 m. This would seem to imply that the large-amplitude topographic waves are not being forced locally but are propagating into the area along rays from a source region farther downstream. We are unaware of any direct observations of topographic wave forcing by the Gulf Stream; however, aside from being the logical energy source for these disturbances, there is mounting indirect evidence that these waves can be forced by large meanders (Hogg, 1981) and also by Gulf Stream rings (Louis and Smith, 1982).

At periods shorter than approximately 16 days, deep front displacements at depth $\geq$2000 m are coherent with near-surface path displacements near the northern edge of the Gulf Stream, and in the 14-day and 5-day period bands these displacements are

associated with spatially coherent, cross-stream velocity fluctuations. Farther offshore within the Gulf Stream, however, the temperature field is generally weakly coherent vertically, and in certain bands (e.g. at periods of 14 days and 4 days) the velocity eigenfunctions also indicate a weak vertical coupling there. This suggests that the deep meandering motions have relatively short cross-stream scales, on the order of a deformation radius (~40 km) or less. The vertically-coherent, organized motion does not occur near the center of the deep jet, but is found near the northern edge of the current, under the region of maximum baroclinicity. Longer-term measurements combining IES and current meter instrumentation are planned to refine the present observations and to provide a detailed description of the regional energetics.

Acknowledgments. The field work and analysis were supported by the Office of Naval Research under contract N00014-81C-0062 and by the National Science Foundation under Grant OCE82-01222 to the University of Rhode Island. One of the authors (W.E.J.) was also supported by the Office of Naval Research under contract N00014-80C-0042 to the University of Miami while writing this manuscript. We wish to thank the Captain and crew of the *R/V Endeavor* for their efforts on several cruises to the survey area, and the University of Rhode Island Technical Services group for their able assistance and support.

APPENDIX

EOF Velocity hodographs

At each site, the EOF analysis yields modes which are defined by the normalized amplitude of each velocity component, $(|u|,|v|)$, and the relative phase of velocity components, (ϕ_u,ϕ_v). The velocity fluctuation described by a given mode may be written as:

$$u = \hat{u} \sin(\omega t + \phi_u)$$

$$v = \hat{v} \sin(\omega t + \phi_v)$$

where $\hat{u}$, $\hat{v}$ are the *dimensional* velocity component amplitudes obtained by rescaling $|u|$ and $|v|$ by the corresponding spectral levels. The major and minor axes of the velocity hodograph are found by defining the quantity $w = (u^2 + v^2)^{1/2}$ and searching for the maximum and minimum of w^2, as a function of ωt:

$$dw^2/d(\omega t) = 0 = -a^2 \cos \omega t \sin \omega t + b^2 \cos \omega t \sin \omega t + c^2(\cos^2 \omega t - \sin^2 \omega t)$$

where

$$a^2 = (\hat{u}^2 \sin^2 \phi_u + \hat{v}^2 \sin^2 \phi_v)$$

$$b^2 = (\hat{u}^2 \cos^2 \phi_u + \hat{v}^2 \cos^2 \phi_v)$$

$$c^2 = 2(\hat{u}^2 \cos \phi_u \sin \phi_u + \hat{v}^2 \cos \phi_v \sin \phi_v)$$

Therefore,

$$\tan^2 \omega t + [(a^2 - b^2)/c^2] \tan \omega t - 1 = 0.$$

The ωt values which maximize or minimize w^2 are found by applying the quadratic formula:

$$\omega t_{\max,\min} = \tan^{-1}\left[-B/2 \pm (B^2 + 4)^{1/2}/2\right],$$

where $B = (a^2 - b^2)/c^2$. The relative phase of the major axis velocity component is $\omega t_{\max}$, and the major and minor axes of the velocity hodograph are obtained by substituting these ωt roots into the expression for w. Finally, the geographic orientation of the major axis is given by:

$$\theta = \tan^{-1}\left[v(\omega t_{\max})/u(\omega t_{\max})\right].$$

REFERENCES

Bryden, H. L. 1976. Horizontal advection of temperature for low-frequency motions. Deep-Sea Res., *23,* 1165–1177.

Casagrande, C. E. 1983. Blake Plateau: near bottom current/temperature measurements on 36°N. Final Report, General Oceanics, Inc., Miami, Florida.

Cornillon, P. 1982. The edge of the Gulf Stream: satellite versus inverted echo sounder determinations. EOS Trans. AGU, *63,* 363.

Groves, G. W. and E. J. Hannan. 1968. Time series regression of sea level on weather. Rev. Geophys., *6,* 129–174.

Halkin, D. and H. T. Rossby. 1985. The structure and transport of the Gulf Stream at 73°W. J. Phys. Oceanogr., *15,* 1439–1452.

Hall, M. M. and H. L. Bryden. 1985. Profiling the Gulf Stream with a current meter mooring. Geophys. Res. Lett., *12,* 203–206.

Halliwell, G. R., Jr. and C. N. K. Mooers. 1983. Meanders of the Gulf Stream downstream from Cape Hatteras 1975–78. J. Phys. Oceanogr., *13,* 1275–1292.

Hansen, D. V. 1970. Gulf Stream meanders between Cape Hatteras and the Grand Banks. Deep-Sea Res., *17,* 495–511.

Hendry, R. M. 1982. On the structure of the deep Gulf Stream. J. Mar. Res., *40,* 119–142.

Hogg, N. G. 1981. Topographic waves along 70W on the Continental Rise. J. Mar. Res., *39,* 627–649.

—— 1983. A note on the deep circulation of the western North Atlantic: its nature and causes. Deep-Sea Res., *30,* 945–961.

Hogg, N. G. and H. Stommel. 1985. On the relation between the deep circulation and the Gulf Stream. Deep-Sea Res., *32,* 1181–1193.

Johns, W. E. 1984. Dynamics and structure of Gulf Stream meanders northeast of Cape Hatteras. Ph.D. thesis, University of Rhode Island, Kingston, RI, 244 pp.

Johns, W. E. and D. R. Watts. 1985. Gulf Stream meanders: Observations on the deep currents. J. Geophys. Res., *90,* 4819–4832.

Kelley, E. A., G. L. Weatherly and J. C. Evans. 1982. Correlation between surface Gulf Stream and bottom flow near 5000 m. J. Phys. Oceanogr., *12,* 1150–1153.

Knauss, J. A. 1969. A note on the transport of the Gulf Stream. Frederick C. Fuglister Sixtieth Anniversary Volume. Deep-Sea Res., *16* (Suppl), 117–123.

Louis, J. P. and P. C. Smith. 1982. The development of the barotropic radiation field of an eddy over a slope. J. Phys. Oceanogr., *12,* 56–73.

Luyten, J. R. 1977. Scales of motion in the deep Gulf Stream and across the Continental Rise. J. Mar. Res., *35,* 49–74.

Priesendorfer, R. W. 1981. Cumulative probability tables for eigenvalues of random covariance matrices, *in* SIO Ref. Series 81–2, Scripps Inst. of Ocean., La Jolla, CA.

Rhines, P. B. 1970. Edge-, bottom-, and Rossby waves in a rotating stratified fluid. Geophys. Fluid Dyn., *1,* 273–302.

Richman, J. G., C. Wunsch and N. G. Hogg. 1977. Space and time scales of mesoscale motions in the western North Atlantic. Rev. Geophys., *15,* 385–420.

Robinson, A. R., J. R. Luyten and F. C. Fuglister. 1974. Transient Gulf Stream meandering. Part I: An observational experiment. J. Phys. Oceanogr., *4,* 237–255.

Schmitz, W. J., Jr. 1978. Observations of the vertical distribution of low frequency kinetic energy in the western North Atlantic. J. Mar. Res., *36,* 295–310.

Schmitz, W. J., Jr., A. R. Robinson and F. C. Fuglister. 1970. Bottom velocity observations directly under the Gulf Stream. Science, *170,* 1192–1194.

Thompson, R. O. R. Y. 1977. Observations of Rossby waves near Site D. Prog. in Oceanogr., *7,* 1–28.

Thompson, R. O. R. Y. and J. R. Luyten. 1976. Evidence for bottom-trapped topographic Rossby waves from single moorings. Deep-Sea Res., *23,* 629–635.

Wallace, J. M. and R. E. Dickinson. 1972. Empirical orthogonal representation of time series in the frequency domain. Part I: Theoretical considerations. J. Appl. Meteor., *11,* 887–892.

Watts, D. R. and W. E. Johns. 1982. Gulf Stream meanders: Observations on propagation and growth. J. Geophys. Res., *87,* 9467–9476.

Wunsch, C. and B. Grant. 1982. Towards the general circulation of the North Atlantic Ocean. Prog. in Oceanogr., *11,* 1–59.

Received: *15 October, 1985;* revised: *14 April, 1986.*